Analyst

PAPER

Cite this: *Analyst*, 2015, **140**, 7939

Simultaneous electrochemical detection of catechol and hydroquinone based on gold nanoparticles@carbon nanocages modified electrode†

Yi Hong Huang,[a] Jian Hua Chen,*[a,b] Li Jing Ling,[a] Zhen Bo Su,[a] Xue Sun,[a] Shi Rong Hu,[a] Wen Weng,[a,b] Yang Huang,[a] Wen Bing Wu[a] and Ya San He[a]

Received 25th August 2015,
Accepted 6th October 2015

DOI: 10.1039/c5an01738f

www.rsc.org/analyst

In the present study, carbon nanocages (CNCs) decorated with gold nanoparticles (AuNPs) with diameters of 2–5 nm were synthesized by simply mixing their solutions. The sizes of the AuNPs are small enough to diffuse into the inside of the CNCs by electrostatic incorporation and their morphologies were characterized by transmission electron microscopy, X-ray diffraction, energy dispersive spectrometry, Raman spectrometry and ultraviolet visible absorption spectra. The AuNPs@CNCs modified electrode was prepared for simultaneous highly sensitive determination of catechol (CC) and hydroquinone (HQ). This modified electrode demonstrated fantastic eletrochemical catalytic activities towards CC and HQ by cyclic voltammetry and differential pulse voltammetry. The calibration curves showed a linear response between the peak currents and the concentrations of CC and HQ. A wide dynamic detection range of 1.0–250.0 μM and 0.1–200.0 μM with a low detection limits (S/N = 3) of 0.0986 μM and 0.0254 μM can be obtained for CC and HQ respectively. The present method was successfully employed for determination of CC and HQ in a practical sample.

1 Introduction

Catechol (1,2-dihydroxybenzene, CC) and hydroquinone (1,4-dihydroxybenzene, HQ) are two isomers of dihydroxybenzene and often coexist in environmental samples as pollutants with high toxicity and low degradability in the ecological system.[1,2] CC and HQ are widely used as important industrial raw and processed materials,[3] such as in photography, dyes, cosmetics and chemical and pharmaceutical industries. They are, however, difficult to separate and determine due to the similar structures and properties of the dihydroxybenzenes.[4] Accordingly, it is very significant to fabricate a simple, rapid and reliable analytical method for a sensitive and selective determination of CC and HQ in various matrices. In order to solve these problems, much work has been done to separate and determine these isomers, such as high performance liquid chromatography,[5] fluorescence spectroscopy,[6] gas chromatography/mass spectrometry,[7] chemiluminescence,[8] spectrophotometry[9] and electrochemical methods.[10–12] Among these, electrochemical methods have occupied a primary position for their fast response, cheap instrumentation, low cost, simple operation, timesaving, high sensitivity and excellent selectivity.[13] In spite of all these, conventional electrodes can not distinguish the overlap of the isomer oxidation–reduction peaks.[14–16] To solve this problem, a wide range of advanced materials, such as graphene, carbon nanotubes, mesoporous carbon, metal nanoparticles, and their composite materials, have been used as enhanced electrode materials to simultaneously determine CC and HQ.[17–22] However, it is still a challenge to explore novel electrode materials for the simultaneous determination of CC and HQ with wider linear range and higher stability.

Carbon nanomaterials have been the subject for decades due to their unique properties, which benefiting the fundamental studies and practical applications.[23] As a kind of three dimensional (3D) graphitic nanostructured material, carbon nanocages (CNCs) have inspired considerable interest on account of their special well-defined structure, high degree of graphitization and purity, superior electrical, mechanical, and chemical properties and biocompatibility.[23,24] CNCs are nanosized hollow particles with graphitic shells, and have shown their significance in a myriad of applications including rechargeable batteries, hydrogen production and storage, cata-

[a]*College of Chemistry and Environmental, Minnan Normal University, Zhangzhou 363000, China. E-mail: jhchen73@126.com; Fax: +86-596-2520035; Tel: +86-596-2591445*

[b]*Fujian Province University Key Laboratory of Modern Analytical Science and Separation Technology, Minnan Normal University, Zhangzhou 363000, China*

†Electronic supplementary information (ESI) available. See DOI: 10.1039/c5an01738f

lysis, sensing and drug and gene delivery.[25–30] In attempts to fabricate these CNCs, sacrificial templating methods have been demonstrated to introduce a porous structure into the graphitized carbon to obtain the CNCs in this article. That is, fine polymeric or inorganic particles were used as the template for the formation of carbon layers on their surfaces. From such templates with a core/shell structure, nanoporous carbons were obtained by removing the template at the core.[31–34] Herein, we report our work on the synthesis of a high-yield of CNCs by the pyrolysis of ethanol and ferrous oxalate at 550.0 °C for 12.0 h.[35] Therefore, CNCs based material sensors were constructed for detection of CC and HQ in this article.

Composite nanomaterials which are made up of nanocarbons in combination with nanometals have attracted significant attention for their novel optical, electronic and catalytic properties.[36] Noble metal-nanoparticles have shown intensive scientific and technological capacities with their unique chemical, electrical and optical properties.[37,38] In recent years, gold,[39–41] silver,[42,43] platinum[44,45] and palladium[46] nanomaterials have attracted considerable interest and studies in the past two decades. Among these, gold nanomaterials have been successfully applied to fabricate various types of optical, electrochemical, sensors and biosensors owing to their good conductivity, electrocatalytic ability and biocompatibility.[47]

Consequently, the 3D graphitic nanostructures of the CNCs were prepared by a hydrothermal method using ethanol and ferrous oxalate as raw materials. AuNPs with diameters of 2–5 nm were prepared by a $NaBH_4$ reduction method in this case. Finally, a novel and simple method was proposed for the preparation of AuNPs coated CNCs (AuNPs@CNCs) by simply mixing the solution of AuNPs and CNCs. AuNPs@CNCs were found to be a highly enhanced sensing material for fabricating electrochemical sensors since this kind of nanomaterial film may generate synergy of electrochemical properties and thus enhance the sensitivity of the sensors.[48] In this paper, the AuNPs@CNCs were applied to a glassy carbon electrode (GCE) and then employed for electrochemical quantification determination of CC and HQ for the first time. The developed method derived this nanocomposite shows high sensitivity and selectivity towards CC and HQ with a wide linear range from 1.000–250.0 μM and 0.1000–200.0 μM and a detection limit of 0.09860 μM and 0.02540 μM respectively. Additionally, it has been successfully applied to determine CC and HQ content using practical samples with satisfactory results. This paper shows that AuNPs@CNCs material can be used in electrochemical sensors. This research can provide significant help for the study of AuNPs, CNCs and AuNPs@CNCs in the field of electrochemical sensors.

2 Experimental

2.1 Reagents and chemicals

Ethanol was obtained from Shanghai Chemical Reagent Co. Ltd. Chloroauric acid ($HAuCl_4{\cdot}4H_2O$), ferrous oxalate, CC and HQ were purchased from Aladdin Chemical Reagent Co. (China). CC and HQ were stored at 4 °C. All other chemicals used were of analytical grade, without further purification. All the aqueous solutions were prepared with twice-distilled water (18.20 MΩ). The working solutions were freshly prepared by diluting a 0.2 M acetate buffer solution and were used throughout all experiments.

2.2 Apparatus

Electrochemical experiments were performed with a CHI 650D electrochemical workstation (China). A conventional three-electrode system was applied for all the electrochemical experiments, which consisted of an Ag/AgCl saturated KCl as a reference electrode, a platinum wire as an auxiliary electrode, and a bare GCE (3 mm in diameter) or a AuNPs@CNCs modified GCE as a working electrode. The surface morphology of the AuNPs@CNCs film was observed with atomic force microscopy (AFM) images (AFM, CSPM 5500, China). Transmission electron microscopy (TEM) was performed on a JEM-1230 electron microscope (JEOL, Ltd, Japan) at an accelerating voltage of 300 kV. The crystal structures of the samples were characterized by X-ray diffraction with Cu K radiation (XRD, Rigaku Dmax-2000 diffractometer). Raman spectra were recorded on a Renishaw Raman microscope (model RM2000) with laser excitation wavelength of 514.5 nm. Ultraviolet visible (UV-vis) absorption spectra were recorded on a Mapada UV-1800PC (Shanghai Mapada Instruments Co., Ltd, China).

2.3 Synthesis of CNCs, AuNPs and AuNPs@CNCs

The synthesis diagram of AuNPs@CNCs is shown in Scheme 1. CNCs were prepared according to Li's methods;[35] 15.0 mL ethanol and 1.5 g ferrous oxalate were put into a 20.0 mL of stainless-steel autoclave at 550.0 °C for 12.0 h. The temperature of the furnace was increased from room temperature to 550.0 °C over 55.0 min and maintained at 550.0 °C for 12.0 h. After that, the autoclave was allowed to cool to room temperature naturally. The precipitate was obtained and washed with absolute ethanol, hydrochloric acid, and distilled water several times. Then precipitate was dried in a vacuum at 60.0 °C for 5.0 h for further characterization.

The AuNPs were prepared according to the literature.[49] Briefly, 0.6 mL of 1.0 wt% $HAuCl_4$ was added to the 40.0 mL of ultrapure water which was precooled at 4.0 °C, then 0.2 mL of 0.2 M K_2CO_3 was added to the above mixed solution. Under stirring 0.4 mL of 0.5 mg mL^{-1} $NaBH_4$ was added quickly, generally repeated with 5 times until the color became violet and then turned to orange red. This was then stirred for another 5.0 min, until 2–5 nm gold nanoparticles could be obtained.

Synthesis of the AuNPs@CNCs composite: briefly, 3.0 mg of CNCs was put into 600.0 mL of the AuNPs solution for several hours until the wine red color disappeared, and then the CNCs coated AuNPs composite could be obtained.

2.4 Preparation of the electrode

Preparation of the modified electrode: prior to coating, the GCE was successively polished with 1.0 μm, 0.3 μm and

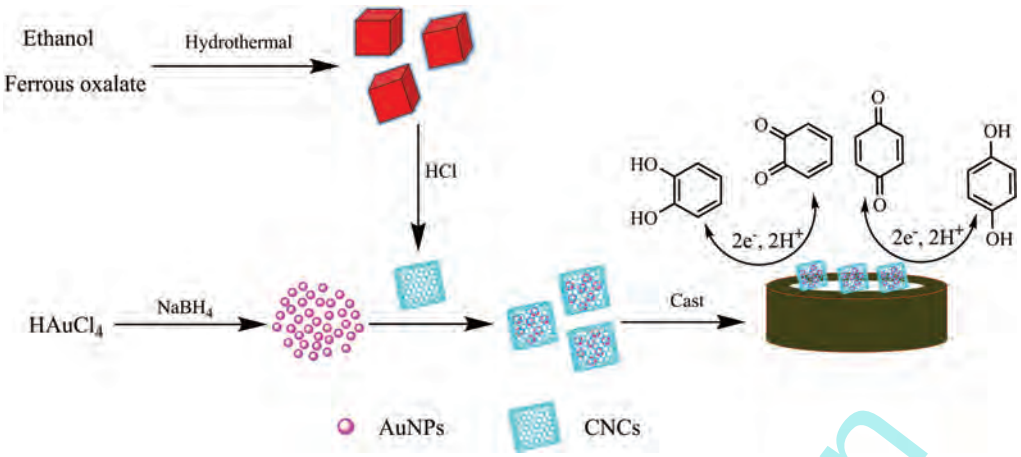

Scheme 1 Illustration of the synthesis of AuNPs@CNCs and the electrochemical oxidization of CC and HQ.

0.05 μm alumina powder and rinsed thoroughly with deionized water, ethanol and then deionized water for several minutes each, and allowed to dry at room temperature. Then the 5.000 μL AuNPs@CNCs aqueous solution (3.000 mg mL^{-1}) was coated on the surface of the GCE and allowed to dry at room temperature to obtain the AuNPs@CNCs composite modified electrode. For comparison, the GCE and CNCs/GCE were prepared by a similar process.

2.5 Operation of electrochemical appliance

The reference electrode, auxiliary electrode and modified electrode were immersed in buffer solutions containing CC and HQ, and then were connected to an electrochemical workstation. Keeping the buffer conditions unchanged, different electrodes were used to compare the electrode peak current. The pH values of the HAc–NaAc buffer solution were varied and the AuNPs@CNCs modified electrode was used to select a best pH value *via* CV. Under the best pH conditions, the AuNPs@CNCs modified electrode was used to test the buffer solution with CC and HQ *via* changing the scan rate during CV. Increased concentrations of CC and HQ in a buffer solution were used to research the linear relationship of the peak current and concentration *via* DPV.

3 Results and discussion

3.1 Characterization of the CNCs, AuNPs and AuNPs@CNCs

The surface morphologies of CNCs, AuNPs and AuNPs@CNCs were examined through TEM and are displayed in Fig. 1. In Fig. 1A, it can be observed that the CNCs have a size of approximately 25 nm. The TEM image of the AuNPs (Fig. 1B) discloses that the size of the AuNPs was approximately 3 nm. The TEM image of AuNPs@CNCs (Fig. 1C) indicates that the AuNPs are well-distributed in the CNCs. More details are presented by Fig. 1D, which shows that the AuNPs are coated on the surface of the CNCs with high-density and uniformity.

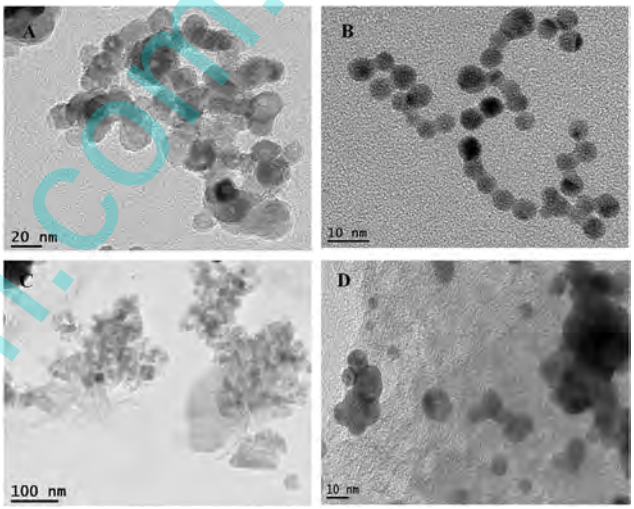

Fig. 1 TEM images of CNCs (A), AuNPs (B) and AuNPs@CNCs (C and D).

XRD analysis was used to verify the formation of the AuNPs@CNCs (Fig. 2A). For pure CNCs, two sharp peaks centered at 22.20° and 44.10° were ascribed to the (002) and (101) diffraction planes of hexagonal graphite (JCPDS card no. 41-1487), suggesting the existence of low crystallinity or disordered graphite on the CNCs. For the AuNPs@CNCs samples, a characteristic peak located at 25.20° was due to the (002) diffraction plane of hexagonal graphite. Peaks located at 38.30° to (111), 44.50° to (200), 64.70° to (220), 77.60° to (311) and 81.70° to (222) planes respectively were observed in the curve of the AuNPs@CNCs, and were consequently marked, demonstrating that the good crystallinity of the AuNPs was dispersed in the CNCs.

The EDS of the AuNPs@CNCs is displayed in Fig. 2B, and indicates that the major element in the AuNPs@CNCs is Au. The inset of Fig. 2B shows the detailed element content of the AuNPs@CNCs.

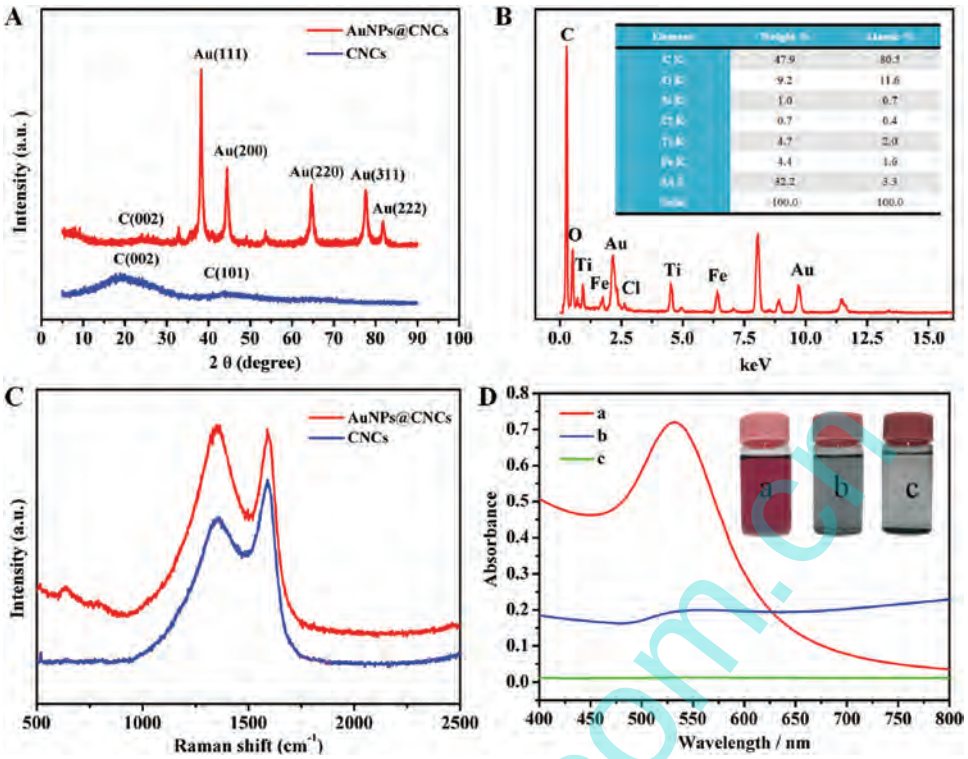

Fig. 2 (A) XRD spectra of the CNCs and AuNPs@CNCs; (B) EDS of AuNPs@CNCs, the inset is detailed element content of the AuNPs@CNCs; (C) Raman spectra of the CNCs and AuNPs@CNCs; (D) UV-vis spectra of the AuNPs solution after complete absorption (a), after absorption of the AuNPs solution for 2 min (b), and the AuNPs solution (c).

As is well known, Raman spectroscopy is a widely used tool to characterize carbon products due to the increase in the Raman intensities by conjugated and double carbon–carbon bonds.[50] Obviously, the two strong Raman peaks at around 1330 cm^{-1} and 1570 cm^{-1} corresponded to the D and G bands of the CNCs and AuNPs@CNCs samples (Fig. 2C). The intensity ratio of the D/G bands reflects the size of the sp^2 domains and the structural disorder of CNCs.[51] In our work, the ratios were calculated to be 0.95 and 1.06 for the CNCs and AuNPs@CNCs, respectively. The enlarged ratio for the AuNPs@CNCs sample confirms the enhanced disorder of the CNCs, owing to the interactions between the Au and CNCs.

The UV-vis spectra of solution after complete absorption of the AuNPs (a), solution of absorption of the AuNPs for 2 min (b), and AuNPs solution (c) are shown in Fig. 2D. It can be observed that the UV spectrum of the AuNPs solution displays a strong absorption peak centered at 532.0 nm (Fig. 2D, curve a), which is the typical characteristic absorbance peak consistent with the reported literature. Curve b displays an absorbance peak of the solution of CNCs which was put into the AuNPs solution for about 2 min, and it is centered at 532.0 nm but is weaker than the absorbance peak of the AuNPs. From curve c, which is the solution after the complete absorption of the AuNPs by CNCs, no obvious absorption peak can be obtained. One can observe that the AuNPs have been decorated on the CNCs.

3.2 Electrochemical behavior of modified electrode

The electrochemical behaviors of 50.00 μM CC and 50.00 μM HQ at bare the GCE, CNCs/GCE and AuNPs@CNCs/GCE were studied by CV. One could observe that in Fig. 3, the CC and HQ could not be separated at the bare electrode. As for the AuNPs/GCE, the redox peak currents for CC were −14.68 μA and 5.580 μA, and for HQ were −4.470 μA and 9.040 μA, respectively. For the CNCs/GCE, two obvious oxidation peaks (0.2330 V and 0.3340 V) and two reduction peaks (0.1780 V and 0.2790 V) can be observed in the voltammogram, suggesting the sensitivity for CC and HQ. The redox peak currents for CC were −19.24 μA and 18.60 μA, and for HQ were −22.99 μA and 13.52 μA, respectively. In addition, the AuNPs@CNC modified electrode also exhibits two obvious redox peaks at 0.2380 V, 0.1710 V and 0.3390 V, 0.2750 V for CC and HQ. The redox peak currents for CC were −36.26 μA and 33.10 μA, for HQ were −39.71 μA and 27.89 μA, respectively, which were higher than that of the CNCs/GCE and AuNPs/GCE. The reasons may be as follows. First, the AuNPs had large specific surface area and high electrical conductivity for promoting a faster electron transfer on the electrode surface. In addition, the CNCs with high degrees of graphitization had excellent electrical conductivity. Moreover, the AuNPs@CNCs composite combines the advantages of AuNPs and CNCs *via* synergism and gave excellent electrical conductivity. This AuNPs@CNCs composite

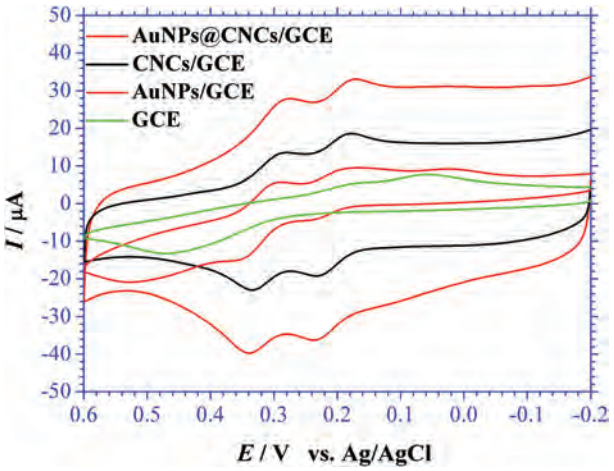

Fig. 3 CVs of 50.00 μM CC and 50.00 μM HQ at the bare GCE, CNCs/GCE, AuNPs/GCE and AuNPs@CNCs/GCE. Scan rate: 0.1000 V s^{-1}.

modified electrode for the electrochemical detection of CC and HQ could enhance the interactions of the CC and HQ molecules to the electrode surface and improve the sensitivity by strong π–π interaction between the AuNPs@CNCs and the CC and HQ isomers. All these results suggested that after the modification of the CNCs with the AuNPs, the AuNPs@CNCs/GCE had excellent electrocatalysis toward CC and HQ.

3.3 Ratio of the CNCs and AuNPs

Three milligrams of the CNCs was added to different masses of the AuNPs solution (200.0, 300.0, 400.0, 500.0, 600.0, 700.0 and 800.0 g) under magnetic stirring for several hours. Then different amounts of AuNPs@CNCs were used in the electrochemical sensor to measure 50.00 μM CC and HQ in pH 5.000 HAc–NaAc solution. The experimental results are shown in Fig. S1.† It can be observed that the oxidation currents of CC and HQ were gradually enhanced in the range of 200.0 g to 600.0 g, and the oxidation current remained almost the same at 600.0 to 800.0 g. This because the hollow CNCs can absorb the AuNPs for formation of the AuNPs@CNCs, and when the mass of the AuNPs solution reached 600.0 g, the hollow CNCs reached a saturated state.

3.4 Influence of the solution pH

In order to optimize the pH, different pH (from 3.000 to 7.000) of HAc–NaAc solutions with 50.00 μM CC and 50.00 μM HQ were prepared. The detailed electrochemical results are shown in Fig. 4A. It can be observed that anodic peak potential (E_{pa}) values of CC and HQ shift negatively with increase of the pH value from 3.000 to 7.000. The peak potentials were proportional to the pH. The regression equations of CC and HQ are E_{pa} (V) = 0.6222 − 0.05590pH (R = 0.9960) and E_{pa} (V) = 0.5321 − 0.05818pH (R = 0.9971). The maximum oxidation peak currents of CC and HQ are found at about pH 5.000, and the results can be observed in the Fig. S2.† These changes can be attributed to the proton involvement in the electrochemical reaction. Additionally, the electrochemical reaction becomes more difficult at a high pH value, owing to the lack of protons. Furthermore, CC and HQ can easily turn into anions at a high pH, generating an electrostatic repulsion between the dihydroxybenzene isomers and the AuNPs@CNCs/GCE, which may result in the peak current decrease.[52] Accordingly, pH 5.000 was chosen as the optimized value for the electrochemical detection of CC and HQ.

3.5 Effects of scan rate

The influence of the scan rate on the AuNPs@CNCs/GCE was investigated by CV and is shown in Fig. 5A. In the 50.00 μM CC and 50.00 μM HQ with pH 5.000 HAc–NaAc solution, with the increase of scan rate, the oxidation peak potential shifted positively and the reduction peak potential shifted negatively. It also can be found that with the increase of scan rate, the redox peak currents of CC and HQ increased linearly with the square root of the scan rate. As shown in Fig. 5B, the regression equations of CC and HQ were I_{pa} (μA) = 63.32 + 0.7892$\nu^{1/2}$ (V s^{-1}, R = 0.9975) and I_{pc} (μA) = −50.68 − 0.7880$\nu^{1/2}$ (V s^{-1}, R = 0.9969); I_{pa} (μA) = 63.32 + 0.7892$\nu^{1/2}$ (V s^{-1}, R = 0.9975) and

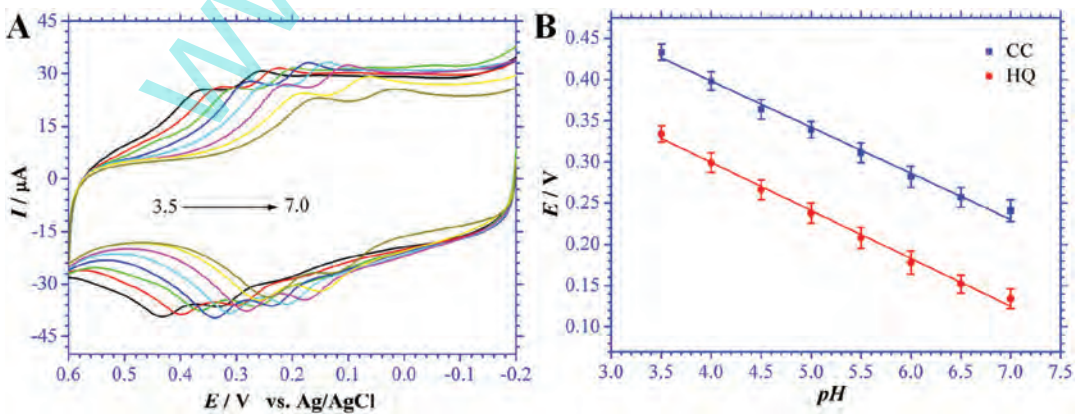

Fig. 4 CVs at the AuNPs@CNCs/GCE with different pH and 50.00 μM CC and 50.00 μM HQ (A); the plots of the anodic peak potential *vs.* the pH values (B). Scan rate: 0.1000 V s^{-1}.

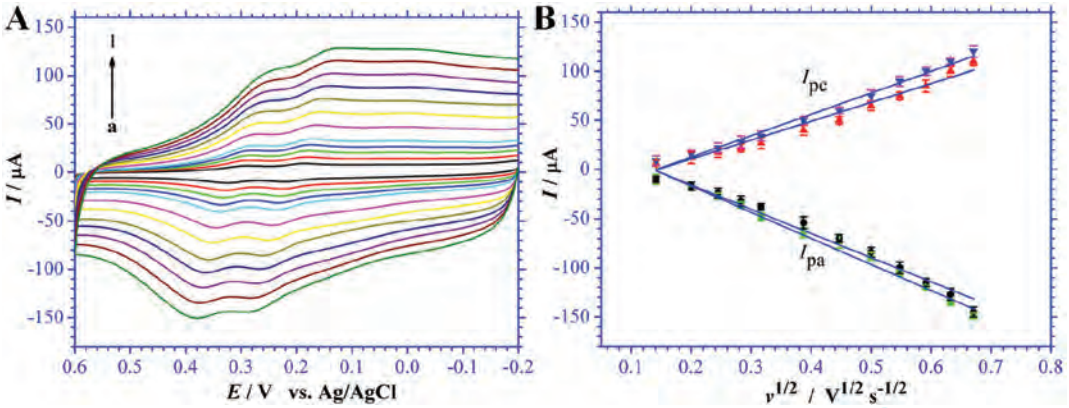

Fig. 5 (A) CVs of the 50.00 μM CC and 50.00 μM HQ at the AuNPs@CNCs/GCE in pH 5.000 HAc–NaAc solution at different scan rates (a–l): 0.02, 0.04, 0.06, 0.08, 0.10, 0.15, 0.20, 0.25, 0.30, 0.35, 0.40, 0.45, 0.50 V s^{-1}; (B) peak potential and peak current vs. the square root of the scan rate.

I_{pc} (μA) = −50.68 − 0.7880$v^{1/2}$ (V s^{-1}, R = 0.9969), respectively. This suggests that the redox reactions of CC and HQ at AuNPs@CNCs modified electrode were typical diffusion-controlled processes. Therefore the probable mechanism of the electrode reaction for CC and HQ was gradually changed from the absorption of CC and HQ at the modified electrode surface into the diffusion onto the electrode surface.

To further characterize the kinetic parameters, the influence of the scan rate on the redox peak potential for CC and HQ was also investigated by CV methods. In Fig. 5A, it can be observed that the oxidation peak potential shifted positively and the reduction peak potential shifted negatively with the increase of scan rate, and the E_{pa} and cathodic peak potential (E_{pc}) showed a linear dependence to the logarithm of scan rate (log v). The linear regression equations for CC were E_{pa} (V) = 0.3079 + 0.07341 log v (V s^{-1}, R = 0.9949) and E_{pc} (V) = 0.1194 − 0.05554 log v (V s^{-1}, R = 0.9847), while for HQ, the linear relationship equations were E_{pa} (V) = 0.4002 + 0.06423 log v (V s^{-1}, R = 0.9846) and E_{pc} (V) = 0.2282 − 0.05381 log v (V s^{-1}, R = 0.9825). On the basis of Laviron's model,[53] the relationship between the potential and the scan rate can be expressed as $2.3RT/(1-\alpha)nF$ (eqn (1)) and $-2.3RT/\alpha nF$ (eqn (2)). Accordingly, the electron-transfer coefficient (α) and electron-transfer number (n) can be calculated; for CC these were 0.5693 and 2, and for HQ were 0.5441 and 2. According to eqn (3), the apparent heterogeneous electron transfer rate constant (k_s) for CC and HQ can be estimated to be 1.207 s^{-1} and 1.576 s^{-1}, respectively, which were higher than those for the bare GCE for CC and HQ (0.02819 s^{-1} and 0.05132 s^{-1}).

$$E_{pa} = E^{0\prime} + \frac{2.3RT}{(1-\alpha)nF}\log v \quad (1)$$

$$E_{pc} = E^{0\prime} - \frac{2.3RT}{\alpha nF}\log v \quad (2)$$

$$\log k_s = \alpha\log(1-\alpha) + (1-\alpha)\log\alpha - \log\frac{RT}{nFv} - \frac{(1-\alpha)\alpha nF\Delta E_p}{2.3RT} \quad (3)$$

3.6 Electrochemical determination of CC and HQ on the AuNPs@CNCs/GCE

DPV possesses higher current sensitivity and better resolution than CV. This was carried out on a AuNPs@CNCs/GCE by increasing the concentration of one isomer while keeping the concentration of the other isomer constant at 50.00 μM, the results of which are displayed in Fig. 6. Under the optimized conditions, it can be seen that the peak currents of CC not only gradually increased with the concentration of CC (Fig. 6A), but also show a linear relationship between each other (Fig. 6B). The corresponding linear regression equations in the two different concentration intervals 1.000–50.00 μM and 50.00–300.0 μM are expressed in eqn (4) and (5). The detection limit was estimated to be 0.09860 μM for CC at a signal-to-noise (S/N) ratio of 3σ (where σ is the standard deviation of a blank solution, n = 7).

$$I_{pa} = -53.46 - 0.2911c \ (R = 0.9983) \quad (4)$$

$$I_{pa} = -64.36 - 0.0712c \ (R = 0.9992) \quad (5)$$

Similarly, Fig. 6C shows the DPV of different concentrations of HQ in the presence of 50.00 μM CC. The anodic peak currents of CC increase linearly with the CC concentration over two concentration intervals of 0.1000–20.00 μM and 20.00–200.0 μM (Fig. 6D). The corresponding linear regression equations are given in eqn (6) and (7), and the detection limit was 0.02540 μM (S/N = 3).

$$I_{pa} = -64.97 - 0.3562c \ (R = 0.9993) \quad (6)$$

$$I_{pa} = -71.13 - 0.0878c \ (R = 0.9987) \quad (7)$$

In addition, the DPV of simultaneously increasing concentrations of CC and HQ was also researched and the result is shown in Fig. 6E. This showed that the peak currents of CC and HQ linearly decreased with increased concentrations of CC and HQ (Fig. 6F), and the corresponding linear regression equations are given in eqn (8) and (9). All the experimental results demonstrated that the AuNPs@CNCs/GCE was good for

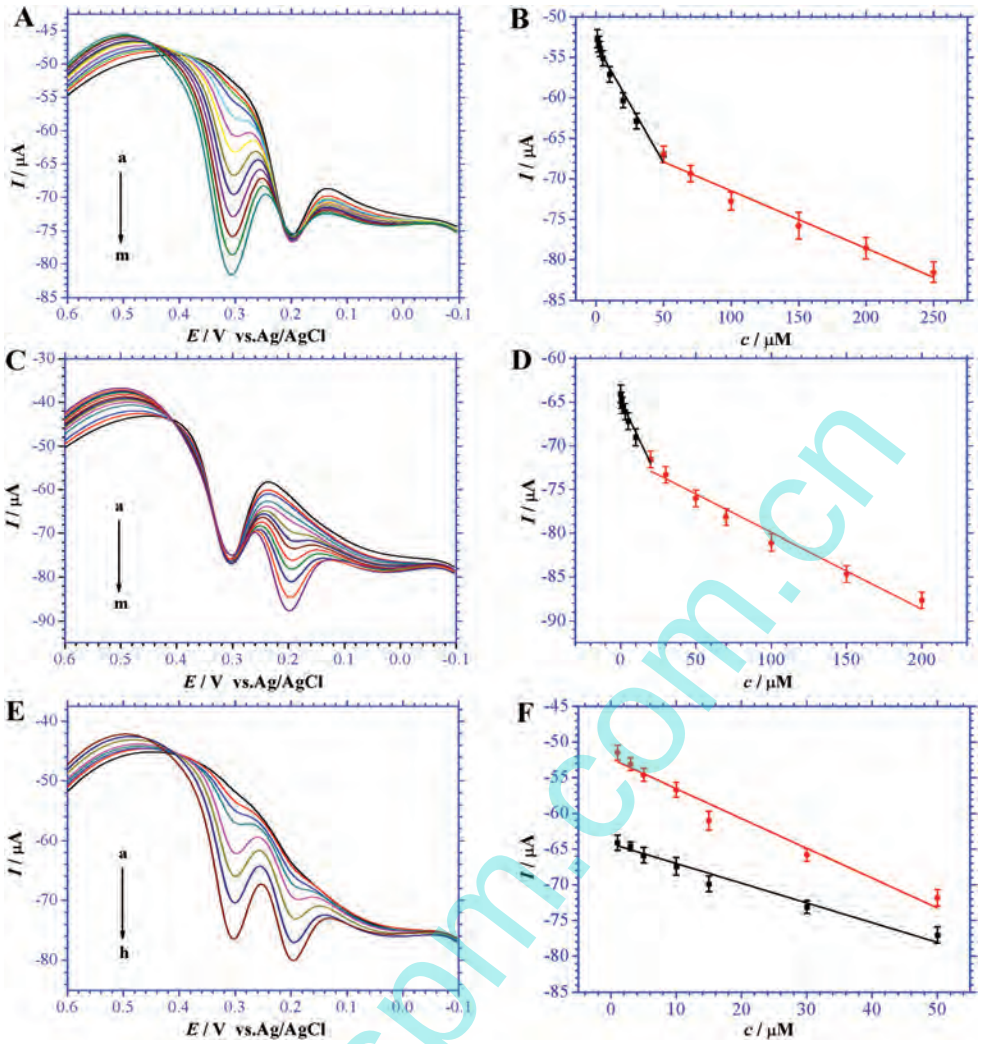

Fig. 6 (A) DPV curves of the AuNPs@CNCs/GCE with different concentrations of CC (from a to m: 1, 2, 3, 5, 10, 20, 30, 50, 70, 100, 150, 200 and 250 μM) in the presence of 50.00 μM HQ; (B) peak current response *vs.* CC concentration; (C) DPV curves of the AuNPs@CNCs/GCE with different concentrations of HQ (from a to m: 0.1, 0.5, 1, 3, 5, 10, 20, 30, 50, 70, 100, 150 and 200 μM) in the presence of 50.00 μM CC; (D) peak current response *vs.* HQ concentration; (E) DPV curves of the AuNPs@CNCs/GCE with different concentrations of CC and HQ (from a to h: 1, 3, 5, 10, 15, 30, 50 and 100 μM); (F) peak current response *vs.* CC and HQ concentrations.

sensitive simultaneous determination of the two dihydroxybenzene isomers without interference of each other. In addition, a comparison with previous literature is displayed in Table 1.

$$I_{pa} = -64.27 - 0.2759c \ (R = 0.9836) \quad (8)$$

$$I_{pa} = -52.35 - 0.4180c \ (R = 0.9849) \quad (9)$$

3.7 Reproducibility and stability of the AuNPs@CNCs/GCE

The reproducibility and stability of the AuNPs@CNCs/GCE were further investigated. The electrode test was performed every two days. The results can be observed in Fig. S3;† the oxidation peak currents of CC and HQ remained almost unchanged, which indicated that the modified electrode had good stability. Five AuNPs@CNCs/GCEs were prepared and investigated by comparing the CV peak currents of 100.0 μM HQ and 100.0 μM CC in a mixture solution, and the relative standard deviations (RSDs) were calculated to be about 3.840% for HQ and 3.920% for CC, which indicated the good reproducibility of the AuNPs@CNCs/GCE. All these data demonstrated that the AuNPs@CNCs composite material modified electrode had a good stability and reproducibility for determination of CC and HQ.

3.8 Interference study

The potential influence of various substances was also investigated to assess the selectivity of the proposed sensor for the determination of CC and HQ. Under the optimal conditions, 50.0-fold resorcinol, phenol and nitrophenol, 400.0-fold of K^+, Na^+, 100.0-fold of Ca^{2+}, Ni^{2+}, Zn^{2+}, Fe^{2+}, Fe^{3+}, Cu^{2+}, Al^{3+}, Mg^{2+}, Cl^-, SO_4^{2-} were performed on CC and HQ determination, and

Table 1 Comparison of different material modified electrodes for determination of CC and HQ

Materials	Concentration (mg mL^{-1})	Volume (μL)	Linear range (μM)		LOD (μM)		Ref.
			CC	HQ	CC	HQ	
Graphene-chitosan	3	5	1–400	1–300	0.75	0.75	18
RGO-MWNTs	2	8	5.5–540	8–391	1.8	1.8	21
CNNS-CNT	2	5	1–200	1–250	0.09	0.13	54
Pyrrolic-NG	—	5	5–200	5–200	1	0.38	55
AuNPs@CNCs	3	5	1.0–300	0.1–200	0.0986	0.0254	This work

Table 2 Experimental results for determination of CC and HQ in wastewater

Wastewater	Found (μM)		Added (μM)		Total (μM)		Recovery (%)		RSD (%)	
	CC	HQ	CC	HQ	CC	HQ	CC	HQ	CC	HQ
1	1.31	0.82	5.000	5.000	6.221	5.952	98.59	102.3	3.42	3.73
2	1.25	0.87	20.00	20.00	20.81	20.41	97.93	97.80	2.55	2.56
3	1.22	0.85	100.0	100.0	100.4	101.1	99.19	100.2	3.03	2.84
4	1.35	0.79	150.0	150.0	152.9	148.8	101.0	98.68	3.15	3.57

it show no interference with the determination (signal change below 5.000%). This demonstrated that the AuNPs@CNCs modified electrode exhibited excellent selectivity for determination of CC and HQ without interference from other coexisting substances.

3.9 Real sample analysis

The practical applicability of this sensor was examined by determination of wastewater for quantitative analysis. The wastewater was filtered and centrifugated to remove any precipitates. Each sample solution was spiked with a certain concentration of CC and HQ. The analysis of the prepared samples was achieved by the standard addition method. The recovery and precision were determined by three replicate measurements for each concentration. The experimental results are shown in Table 2. It can be observed that the recovery ranges for CC and HQ were about 97.93–101.0%, and 97.80–102.3%, respectively. This result shows a good accuracy. Therefore, the AuNPs@CNCs modified electrode can be used for the simultaneous determination of CC and HQ.

4 Conclusions

In conclusion, a new type of electrochemical sensor for the determination of CC and HQ based on AuNPs@CNCs was proposed. Combining the advantages of both the excellent conductivity of the AuNPs and the nanostructure of the CNCs, the AuNPs@CNCs modified electrode could enhance the interactions of the CC and HQ molecules to the electrode surface and improve the detection sensitivities by strong π–π interaction or favorable electrostatic attraction between the AuNPs and CNCs. The characterization results showed that the AuNPs were well dispersed in the composite CNCs. This flexible sensor with many outstanding merits such as low detection limits, excellent sensitivity, unique selectivity and stability has promising perspectives in the field of flexible electronics.

Acknowledgements

This work was supported by National Natural Science Foundation of China (no. 21076174 and no. 21175115), National Natural Science Foundation of Fujian (2012J06005 and 2014J01051), and the science and technology foundation of Fujian provincial bureau quality and technical supervision (no. FJQI2012029, no. FJQI2013108). The authors also thank the anonymous referees for comments on this manuscript.

References

1 X. Wang, M. Wu, H. Li, Q. Wang, P. He and Y. Fang, *Sens. Actuators, B*, 2014, **192**, 452–458.
2 Q. Guo, J. Huang, P. Chen, Y. Liu, H. Hou and T. You, *Sens. Actuators, B*, 2012, **163**, 179–185.
3 L. Wang, Y. Zhang, Y. Du, D. Lu, Y. Zhang and C. Wang, *J. Solid State Electrochem.*, 2012, **16**, 1323–1331.
4 S. Dong, P. Zhang, Z. Yang and T. Huang, *J. Solid State Electrochem.*, 2012, **16**, 3861–3868.
5 S. Pati, P. Crupi, I. Benuccic, D. Antonacci, A. Di Luccia and M. Esti, *Food Res. Int.*, 2014, **66**, 207–215.
6 Z. Li, R. Sun, Y. Ni and S. Kokot, *Anal. Methods*, 2014, **6**, 7420–7425.
7 E. L. B. Lourenço, A. Ferreira and E. Pinto, *Chromatographia*, 2006, **63**, 175–179.
8 Q. Lu, H. Hu, Y. Wu, S. Chen, D. Yuan and R. Yuan, *Biosens. Bioelectron.*, 2014, **60**, 325–331.

9 R. Sun, Y. Wang, Y. Ni and S. Kokot, *J. Hazard. Mater.*, 2014, **266**, 60–67.
10 H. Yin, Q. Zhang, Y. Zhou, Q. Ma, T. Liu, L. Zhu and S. Ai, *Electrochim. Acta*, 2011, **56**, 2748–2753.
11 Y. Zhang, S. Xiao, J. Xie, Z. Yang, P. Pang and Y. Gao, *Sens. Actuators, B*, 2014, **204**, 102–108.
12 B. Nasr, G. Abdellatif, P. Canizares, C. Saez, J. Lobato and M. A. Rodrigo, *Fullerenes, Nanotubes, Carbon Nanostruct.*, 2015, **23**, 410–417.
13 X. Zhou, Z. He, Q. Lian, Z. Li, H. Jiang and X. Lu, *Sens. Actuators, B*, 2014, **193**, 198–204.
14 L. Wang, Y. Meng, Q. Chen, J. Deng, Y. Zhang, H. Li and S. Yao, *Electrochim. Acta*, 2013, **92**, 216–225.
15 Q. Guo, J. Huang, P. Chen, Y. Liu, H. Hou and T. You, *Sens. Actuators, B*, 2012, **163**, 179–185.
16 X. Yue, S. Pang, P. Han, C. Zhang, J. Wang and L. Zhang, *Electrochem. Commun.*, 2013, **34**, 356–359.
17 H. Du, J. Ye, J. Zhang, X. Huang and C. Yu, *J. Electroanal. Chem.*, 2011, **650**, 209–213.
18 H. Yin, Q. Zhang, Y. Zhou, Q. Ma, T. Liu, L. Zhu and S. Ai, *Electrochim. Acta*, 2011, **56**, 2748–2753.
19 L. Tang, Y. Zhou, G. Zeng, Z. Li, Y. Liu, Y. Zhang, G. Chen, G. Yang, X. Lei and M. Wu, *Analyst*, 2013, **138**, 3552–3560.
20 Y. Quan, Z. Xue, H. Shi, X. Zhou, J. Du, X. Liu and X. Lu, *Analyst*, 2012, **137**, 944–952.
21 F. Hu, S. Chen, C. Wang, R. Yuan, D. Yuan and C. Wang, *Anal. Chim. Acta*, 2012, **724**, 40–46.
22 B. Unnikrishnan, P. L. Ru and S. M. Chen, *Sens. Actuators, B*, 2012, **169**, 235–242.
23 Y. Li, C. Zhou, X. Xie, G. Shi and L. Qu, *Carbon*, 2010, **48**, 4190–4196.
24 K. H. Lim, H. S. Oh and H. Kim, *Electrochem. Commun.*, 2009, **11**, 1131–1134.
25 X. Lou, L. Archer and Z. Yang, *Adv. Mater.*, 2008, **20**, 3987–4019.
26 R. Zhang, M. Hummelgård and H. Olin, *Carbon*, 2010, **48**, 424–430.
27 H. Li, Q. Yue, S. Xu, L. Wang and J. Liu, *Mater. Lett.*, 2012, **66**, 353–356.
28 S. Teng, X. Wang, B. Xia and J. Wang, *J. Power Sources*, 2010, **195**, 1065–1070.
29 Y. Ma, Z. Hu, K. Huo, Y. Lu, Y. Hu, Y. Liu, J. Hu and Y. Chen, *Carbon*, 2005, **43**, 1667–1672.
30 A. Vinu, M. Miyahara, T. Mori and K. Ariga, *J. Porous Mater.*, 2006, **13**, 379–383.
31 B. Y. Xia, J. N. Wang, X. X. Wang, J. J. Niu, Z. M. Sheng, M. R. Hu and Q. C. Yu, *Adv. Funct. Mater.*, 2008, **18**, 1790–1798.
32 H. Tamai, T. Sumi and H. Yasuda, *J. Colloid Interface Sci.*, 1996, **177**, 325–328.
33 S. Yoon, K. Sohn, J. Kim, C. Shin and J. Yu, *Adv. Mater.*, 2002, **14**, 19–21.
34 T. W. Kim, I. S. Park and R. Ryoo, *Angew. Chem., Int. Ed.*, 2003, **115**, 4511–4515.
35 G. Li, H. Yu, L. Xu, Q. Ma, C. Chen, Q. Hao and Y. Qian, *Nanoscale*, 2011, **3**, 3251–3257.
36 C. L. Sun, H. H. Lee, J. M. Yang and C. C. Wu, *Biosens. Bioelectron.*, 2011, **26**, 3450–3455.
37 X. Wang, M. Wu, W. Tang, Y. Zhu, L. Wang, Q. Wang, P. He and Y. Fang, *J. Electroanal. Chem.*, 2013, **695**, 10–16.
38 T. Qian, C. Yu, X. Zhou, S. Wu and J. Shen, *Sens. Actuators, B*, 2014, **193**, 759–763.
39 C. M. Cobley, J. Y. Chen, E. C. Cho, L. V. Wang and Y. N. Xia, *Chem. Soc. Rev.*, 2011, **40**, 44–56.
40 E. Koposova, G. Shumilova, Y. Ermolenko, A. Kisner, A. Offenhäusser and Y. Mourzina, *Sens. Actuators, B*, 2014, **207**, 1045–1052.
41 E. G. Pineda, F. Alcaide, M. J. R. Presa, A. E. Bolzan and C. A. Gervasi, *ACS Appl. Mater. Interfaces*, 2015, **7**, 2677–2687.
42 J. Tashkhourian, M. R. H. Nezhad, J. Khodavesi and S. Javadi, *J. Electroanal. Chem.*, 2009, **633**, 85–91.
43 W. N. Hu, D. M. Sun and W. Ma, *Electroanalysis*, 2010, **22**, 584–589.
44 U. Yogeswaran, S. Thiagarajan and S. M. Chen, *Anal. Biochem.*, 2007, **365**, 122–131.
45 S. Thiagarajan and S. M. Chen, *Talanta*, 2007, **74**, 212–222.
46 K. Yoshii, Y. Oshino, N. Tachikawa, K. Toshima and Y. Katayama, *Electrochem. Commun.*, 2014, **52**, 21–24.
47 X. Tian, C. Cheng, H. Yuan, J. Du, D. Xiao, S. Xie and M. M. F. Choi, *Talanta*, 2012, **93**, 79–85.
48 L. Zhou, J. Wang, D. Li and Y. Li, *Food Chem.*, 2014, **162**, 34–40.
49 M. Wei, L. G. Sun, Z. Y. Xie, J. F. Zhii, A. Fujishima, Y. Einaga, D. G. Fu, X. M. Wang and Z. Z. Gu, *Adv. Funct. Mater.*, 2008, **18**, 1414–1421.
50 F. Gao, X. Cai, X. Wang, C. Gao, S. Liu, F. Gao and Q. Wang, *Sens. Actuators, B*, 2013, **186**, 380–387.
51 R. C. de Guzman, J. Yang, M. M. C. Cheng, S. O. Salley and K. Y. Simon Ng, *J. Power Sources*, 2014, **246**, 335–345.
52 W. Si, W. Lei, Y. Zhang, M. Xia, F. Wang and Q. Hao, *Electrochim. Acta*, 2012, **85**, 295–301.
53 E. Laviron, *J. Electroanal. Chem.*, 1979, **101**, 19–28.
54 H. Zhang, Y. Huang, S. Hu, Q. Huang, C. Wei, W. Zhang, W. Yang, P. Dong and A. Hao, *Electrochim. Acta*, 2015, **176**, 28–35.
55 H. L. Guo, S. Peng, J. H. Xu, Y. Q. Zhao and X. Kang, *Sens. Actuators, B*, 2014, **193**, 623–629.